Hindawi Publishing Corporation
Journal of Nanomaterials
Volume 2016, Article ID 3145912, 8 pages
http://dx.doi.org/10.1155/2016/3145912

Research Article

The Effect of Calcination Temperature on Structure and Photocatalytic Properties of WO_3/TiO_2 Nanocomposites

Joanna Mioduska, Anna Zielińska-Jurek, Marcin Janczarek, and Jan Hupka

Department of Chemical Technology, Faculty of Chemistry, Gdansk University of Technology, 80-233 Gdansk, Poland

Correspondence should be addressed to Anna Zielińska-Jurek; annjurek@pg.gda.pl

Received 5 April 2016; Revised 16 June 2016; Accepted 5 July 2016

Academic Editor: Jim Low

Series of WO_3/TiO_2 nanocomposites were obtained by hydrothermal method followed by calcination in the temperature range from 400°C to 900°C. The characteristics of photocatalysts by X-ray diffractometry (XRD), scanning electron microscope (SEM), and diffuse reflectance spectroscopy (DRS) showed that increasing the calcination temperature from 400 to 900°C resulted in change of photocatalytic activity under UV-Vis light. Moreover, the amount of WO_3 crystalline phase and amorphous phase in WO_3/TiO_2 aggregates, as revealed by XRD analysis, was dependent on the calcination temperature. The WO_3/TiO_2 samples with 8 mol% load of WO_3 in respect to TiO_2 calcinated at 500 and 800°C possess the highest photocatalytic activity in reaction of phenol degradation, which is about 1.2 and 1.5 times that with calcination at 400°C. The increase in calcination temperature above 400°C resulted in increase of WO_3 crystallinity and reduction of the amount of amorphous phase in the nanocomposite structure. Moreover, the annealing of nanocomposites above 700°C decreases the value of optical band gap energies of obtained WO_3/TiO_2 nanomaterials.

1. Introduction

Photocatalytic reactions at the surface of titanium(IV) oxide have been used for degradation of hydrocarbons, pesticides and dyes from aquatic systems [1, 2], volatile organic compounds [3] and deactivating bacteria in air [4]. However, the application of TiO_2 for degradation of emerging pollutants from gas and aqueous phases still needs to tackle a variety of scientific problems.

Photocatalytic efficiency of TiO_2 is limited by fast recombination of electron-hole pairs. Additionally, for TiO_2 the band gap is equal to 3.2 eV and 3.0 eV in the anatase and rutile crystalline phase, respectively. It corresponds to a radiation wavelength of 388 nm, which lies in the UVA spectrum of 300 to 388 nm. Therefore, the range of radiation required for excitation of TiO_2-based photocatalysts limits the large-scale application of photocatalysis, because solar spectrum contains only a small part (3–5%) of UV radiation. This is the main force for the development of the second generation of photocatalysts, with photocatalytic activity under the visible range ($\lambda > 400$ nm) and reduced recombination rate between electrons and holes [5].

Photocatalysts can be sensitized for visible light by either doping or chemical surface modification by metals, metal ions, or nonmetals [6–8]. However, research on the second generation has revealed several problems regarding practical aspects of photocatalysis. The first issue is that sensitization of photocatalysts to visible light not always results in an increase of photoactivity and selectivity. Moreover, it even can decrease the photoactivity and selectivity. Photosensitizing TiO_2 with suitable dyes leads to its self-destruction, while nonmetal or metal ion dopants may act as recombination centers of e^- and h^+.

Regarding Emeline et al. [5] the third-generation photoactive materials are based on reducing the band gap of TiO_2 by coupling two different semiconductors which could transfer electrons from an excited band gap semiconductor into another attached one assuming proper conduction band potentials [5]. Such conformation favors separation of photoinduced electrons and holes and improves photocatalytic efficiency of the semiconductor heterostructure.

Recent studies on next generation photocatalysts focused on the coupling of titanium(IV) oxide with tungsten(VI) oxide, a semiconductor with band gap equal to 2.8 eV [9, 10].

The valence and conduction bands of tungsten(VI) oxide are correspondingly lower than in the case of titanium(IV) oxide and the energy band gap is also lower [11, 12]. The combination of these two semiconductors results in enhanced photocatalytic and photochromic potential and accelerates electron transfer from WO_3 to TiO_2. Akurati et al. have observed that the introduction of tungsten to the structure of anatase results in efficient separation of electron-hole pairs, which are formed during irradiation of titanium(IV) oxide [13]. Additionally, combination of these two semiconductors gives the opportunity to obtain a photocatalyst with extended range of optical absorption spectrum [14–16]. However, most of the investigations focused on degradation of dyes in the aqueous phase using WO_3/TiO_2 nanocomposites, but few pertain to the degradation of organic pollutants in the gas phase and aqueous phases.

Recent studies focused on the effect of the particle size and crystallinity on the photocatalytic properties of WO_3/TiO_2 nanocomposites [17, 18]. Crystallinity is one of the critical parameters that influences the photocatalytic performance of photocatalyst. Ohtani et al. reported that amorphous titania plays a role as a recombination center, and it exhibits negligible reactivity in several photocatalytic reactions [19]. However, there is no report in literature concerning the influence of the amorphous fraction of the WO_3/TiO_2 nanocomposites on their photocatalytic activity.

Therefore, the aim of the present paper is systematic study of surface properties of coupled WO_3/TiO_2 nanocomposites and their photocatalytic activity in reaction of phenol degradation under UV-Vis irradiation. Phenol was chosen as a model degradation molecule as it is one of the major pollutants discharged in the wastewater from the various industries that can accumulate in the environment [20]. The influence of calcination temperature in range from 400°C to 900°C on crystallinity, amorphous phase content, and photoactivity for WO_3/TiO_2 nanomaterials is for the first time reported in this paper. Additionally, the effect of precursor and the amount of tungsten(VI) oxide on the photodegradation efficiency was also investigated.

2. Experimental

2.1. Materials and Instruments. All applied reagents were of analytical grade and used without further purification. Titanium(IV) butoxide (≥97%) was supplied by Fluka and used as titanium source for the preparation of TiO_2 nanoparticles. Ammonium metatungstate hydrate was provided by Sigma-Aldrich and used as the starting material for the preparation of tungsten(VI) oxide nanoparticles. Commercial WO_3 nanoparticles were supplied from Sigma-Aldrich and also used for coupling with TiO_2 after hydrolysis unit process.

The crystal structures of the WO_3/TiO_2 nanoparticles were determined from XRD pattern measured in the range of $2\theta = 20–80^\circ$ using X-ray diffractometer (X'Pert PRO-MPD, Philips) with Cu target ($\lambda = 1.542$ Å). The crystallite size was estimated by Scherrer equation using the corrected full width (line-broadening by Cu-$K_{\alpha 2}$ radiation and emanation in the optical path of a diffractometer) at half maximum (FWHM) of the most intense XRD peaks of anatase, rutile, and WO_3 at ca. 25.3° and 27.4° and 23.1° or 24.3°, respectively. A constant of 0.891 in the Scherrer equation was used.

Amorphous content of photocatalysts was calculated by the internal standard method, in which highly crystalline nickel oxide (NiO, Alfa Aesar) was used as the standard, by mixing photocatalyst (80 wt%) and NiO (20 wt%) samples.

Jasco V-670 spectrophotometer equipped with PIN-757 integrating sphere where the baseline was recorded using $BaSO_4$ as a reference was used for characterization of light absorption properties of modified photocatalysts. UV/Vis diffuse reflectance (DR) spectra were recorded, and the data were converted to obtain absorption spectra.

Quanta FEG 250 scanning electron microscope (SEM) was used in the investigation of surface morphologies of WO_3/TiO_2 nanocomposites. Photocatalyst samples were coated with a thin layer of gold using a Leica EM SCD500 coater. EDX analyses were performed for selected representative sample areas.

2.2. Preparation of WO_3/TiO_2 Photocatalysts. The WO_3/TiO_2 photocatalysts were obtained by hydrothermal method, as presented in Figure 1. TiO_2 nanoparticles were prepared by hydrolysis of titanium(IV) butoxide (TBT), which was added dropwise to water and stirred for 30 min. Uniformly mixed commercial WO_3 nanoparticles or ammonium metatungstate (AmT) hydrate was added at room temperature to TiO_2 sol and thoroughly mixed. The hydrothermal reaction took place in a Teflon autoclave at 110°C for 24 h. Precipitated WO_3/TiO_2 particles were centrifuged (3000 rpm), dried at 80°C to dry mass, and calcinated at 400–900°C for 2 h.

2.3. Evaluation of Photocatalytic Activity. The photocatalytic activity of WO_3/TiO_2 powders in the UV-Vis light irradiation was estimated by measuring the decomposition rate of phenol in an aqueous solution. A 25 cm^3 of $2 \cdot 10^{-4}$ M phenol solution containing 0.05 g suspended photocatalyst was stirred using a magnetic stirrer and aerated (5 dm^3/h) prior to and during the photocatalytic process. The suspension was irradiated using a Xenon lamp (6271H, Oriel), with UV-Vis emission range. Measured light flux was (in the range from 310 to 380 nm) 24 mW/cm^2. The photoreactor was equipped with a quartz window and exposure layer thickness was 3 cm. The temperature of the aqueous phase during irradiation was kept at 15°C using water jacket. Aliquots of 1.5 cm^3 of the aqueous suspension were collected at regular time periods during irradiation and filtered through syringe filters ($\varnothing = 0.2\,\mu$m) to remove photocatalyst particles. Phenol concentration was estimated by colorimetric method using a UV-Vis spectrophotometer (DU-7, Beckman). Photocatalytic degradation runs were preceded by blind test in the absence of a photocatalyst or illumination for 1 hour. No degradation of phenol was observed in the absence of either the photocatalyst or illumination.

3. Results and Discussion

The effect of tungsten(VI) oxide amount as well as calcination temperature during preparation route on the photocatalytic

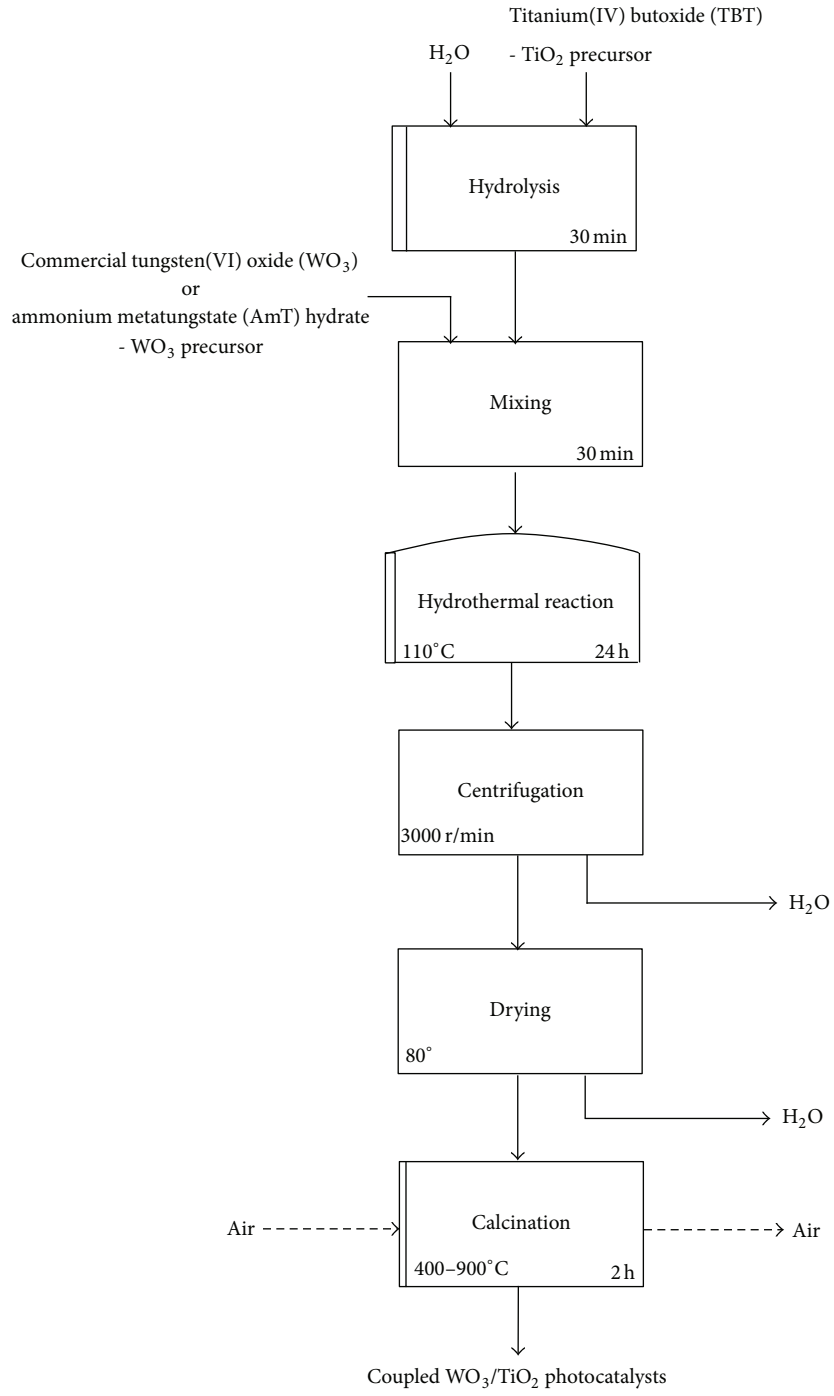

Figure 1: Schematic diagram of the preparation of WO_3/TiO_2 photocatalysts.

activity of obtained WO_3/TiO_2 nanocomposites was investigated. The amount of ammonium metatungstate taken for photocatalyst preparation was calculated on the assumption that the content of WO_3 in the photocatalysts after synthesis should be from 3 to 10 mol% of the photocatalyst dry mass.

3.1. Absorption Properties. Modification of titanium(IV) oxide with tungsten(VI) oxide resulted in increased absorption range in the visible light range. The UV-Vis diffuse reflectance spectra of WO_3/TiO_2 samples prepared with different amounts of ammonium metatungstate (AmT) from 3 to 10 mol% are shown in Figure 2(a). Pure TiO_2 showed absorption threshold at 395 nm. Samples of coupled semiconductors WO_3/TiO_2 exhibited two characteristic light absorption edges in DRS curves. The UV region is attributable to the intrinsic band gap of TiO_2 semiconductor and others in the visible region from 410 nm to 500 nm, related to modification of TiO_2 with WO_3. It was observed that increasing AmT

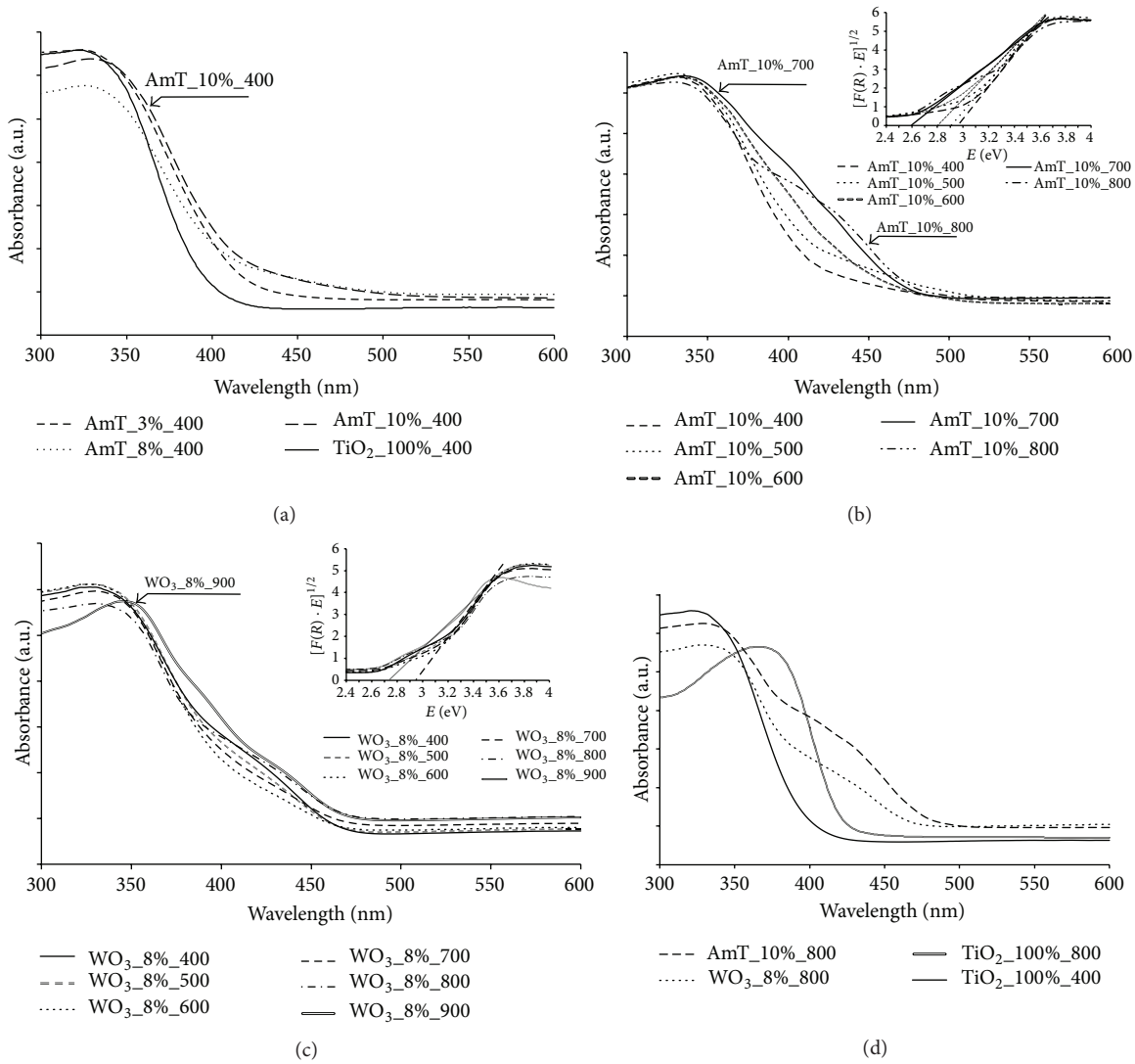

Figure 2: The DR/UV-Vis spectra of WO_3/TiO_2 with different amounts of ammonium metatungstate (a), WO_3/TiO_2 calcinated at 400, 500, 600, 700, and 800°C for TiO_2 modified with AmT (b), determination of indirect interband transition energies for TiO_2 modified with commercial WO_3 (c), and the DR/UV-Vis spectra of pure TiO_2 calcinated at 400°C and 800°C and WO_3/TiO_2 powders with the highest intensity of visible light absorption (d).

amount results in an increase of absorbance in the visible light region.

The effect of the calcination temperature on absorption properties for TiO_2 modified with commercial WO_3 and obtained from precursor (AmT) is shown in Figures 2(b) and 2(c). The red shift in the absorption edge of the WO_3/TiO_2 samples depends on the calcination temperature and the chemical nature of WO_3 (commercial WO_3 particles or WO_3 obtained from AmT precursor). As the calcination temperature increases, the absorption edges of photocatalysts' red-shifts and the absorption intensity in the visible region increase, especially for samples calcinated at most elevated temperatures, that is, at 800 to 900°C.

The DR/UV-Vis spectra of pure TiO_2 calcinated at 400°C and 800°C as well as WO_3/TiO_2 powders with the highest intensity of visible light absorption are presented in Figure 2(d). The greatest increase in the intensity of the visible light absorption was observed for sample AmT_10%_800 containing 10 mol% of WO_3. The obtained results are in accordance with those obtained by other authors [21, 22] showing that the red shift in the absorption edge of the WO_3/TiO_2 nanoparticles results from the formation of defect energy levels and tungsten impurity energy levels in the structure of nanocomposites.

The indirect band gap values of WO_3/TiO_2 photocatalysts are listed in Table 1. The undoped TiO_2 has a band gap of 3.1 eV. As it is evident from Figures 2(a)–2(c), there were changes in absorbance wavelength, which can be correlated to a change in the band gaps of prepared particles.

The determined energy band gaps of WO_3/TiO_2 nanocomposites are lower than that of pure TiO_2 nanoparticles; hence coupled semiconductors extend the range of excitation light, which could result in greater photocatalytic activities under visible light. It can also be observed that the band gap

Table 1: Characteristics of WO_3/TiO_2 nanocomposites. The effect of calcination temperature on energy band gap and photocatalytic properties.

Sample label	WO_3 amount (mol%)	Phenol degradation constant rate $(min^{-1}) \cdot 10^{-2}$	Energy band gap (eV)
TiO_2_100%_400	0	0.75	3.15
TiO_2_100%_800	0	0.66	3.0
WO_3_100%_400	100	0.37	2.65
WO_3_100%_800	100	0.26	2.60
AmT_3%_400	3	0.06	2.95
AmT_5%_400	5	0.15	2.95
AmT_8%_400	8	0.12	2.95
AmT_8%_500	8	0.24	2.95
AmT_8%_600	8	0.32	2.85
AmT_8%_700	8	0.32	2.70
AmT_8%_800	8	0.77	2.75
AmT_10%_400	10	0.21	2.95
AmT_10%_500	10	0.32	2.90
AmT_10%_600	10	0.34	2.80
AmT_10%_700	10	0.39	2.75
AmT_10%_800	10	0.87	2.84
WO_3_5%_300	5	0.87	3.05
WO_3_5%_400	5	0.91	3.05
WO_3_5%_500	5	1.21	3.05
WO_3_5%_600	5	0.66	3.05
WO_3_5%_700	5	0.61	2.95
WO_3_5%_800	5	0.95	2.75
WO_3_8%_400	8	0.84	2.95
WO_3_8%_500	8	1.04	2.98
WO_3_8%_600	8	0.81	2.95
WO_3_8%_700	8	0.67	2.95
WO_3_8%_800	8	1.27	2.95
WO_3_8%_900	8	0.8	2.85
WO_3_10%_400	10	0.56	3.0
WO_3_10%_500	10	0.41	3.0
WO_3_10%_600	10	0.67	3.0
WO_3_10%_700	10	0.39	2.95
WO_3_10%_800	10	0.66	2.85

(E_g) of WO_3/TiO_2 nanocomposites decreases at calcination temperatures above 700°C. Yang et al. [23] reported that formation of defective energy levels decreases the total energy band gap of coupled photocatalysts. The impact of WO_3 contribution to the adjustment energy band gap achieved by coupling TiO_2 nanoparticles with changing percent of WO_3 depends on the source of tungsten in the photocatalyst and its amount [15]. Our observations confirm results presented by Kwon et al. [15]. Moreover, we also found that not only the amount of dopant but also the chosen calcination temperature during preparation procedure influences the energy band gap.

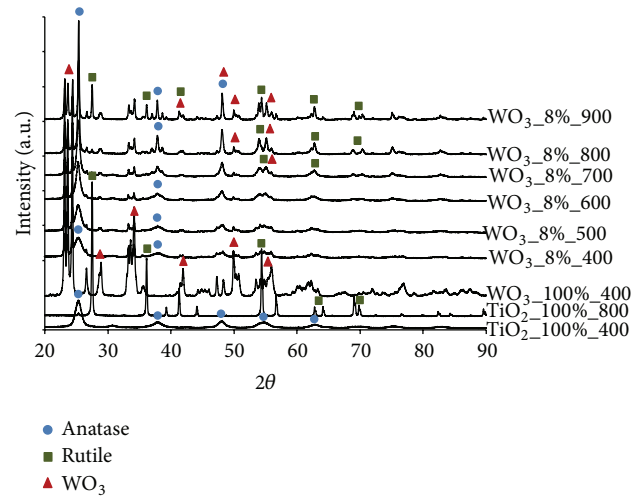

Figure 3: XRD patterns of WO_3/TiO_2 nanoparticles calcinated from 400 to 900°C.

3.2. XRD Analysis. XRD patterns of WO_3/TiO_2 samples of different calcination temperatures are shown in Figure 3(a). The presence of the primary diffraction peaks of TiO_2 at $2\theta = 25.29$, 37.95, 47.97, 54.56, and 62.69 was observed, which can be, respectively, indexed as (101), (103), (200), (105), and (213) planes of anatase phase of titanium(IV) oxide (JCPDS number 21-1272). Pure self-obtained anatase particles transform to rutile at temperature above 700°C. The peaks at 2θ 27.5 (110), 36.1 (101), 56.7 (220), and 64.1 (310), were corresponding to rutile and were observed for TiO_2 sample calcinated at 800°C, regarding phase transition from anatase to rutile. For coupled semiconductors the presence of WO_3 in the structure of nanocomposites results in inhibition of anatase/rutile transformation. The increase of the calcination temperature above 700°C led to an increase of proportion of the rutile phase to anatase in WO_3/TiO_2 samples but not full transformation of anatase to rutile. For WO_3/TiO_2 sample calcinated at 900°C, the ratio of anatase to rutile was 2 : 1.

The signals corresponding to the primary reflections of WO_3 can be observed in the WO_3/TiO_2 samples at $2\theta = 23.1$, 23.7, 24.3, 26.6, 28.7, 33.3, 34.2, and 49.9. These signals can be associated with (001), (020), (200), (120), (111), (021), (220), and (400) planes of the monoclinic phase of WO_3 (JCPDS number 036-0101).

The morphology of WO_3-loaded TiO_2 is strongly influenced by heat treatment procedure. The results presented in Table 2 indicated that below 500°C WO_3/TiO_2 nanocomposites contain a high amorphous phase content (60%) with respect to the crystalline phase content (40%). Further increase in the calcination temperature (from 500 to 900°C) affects the increase in the amount of crystalline phase (80%) and reduction in the amount of amorphous phase (20%) in the nanocomposite structure. This means that for the selected parameters of preparation of WO_3/TiO_2 nanocomposites the calcination is preferably carried out at

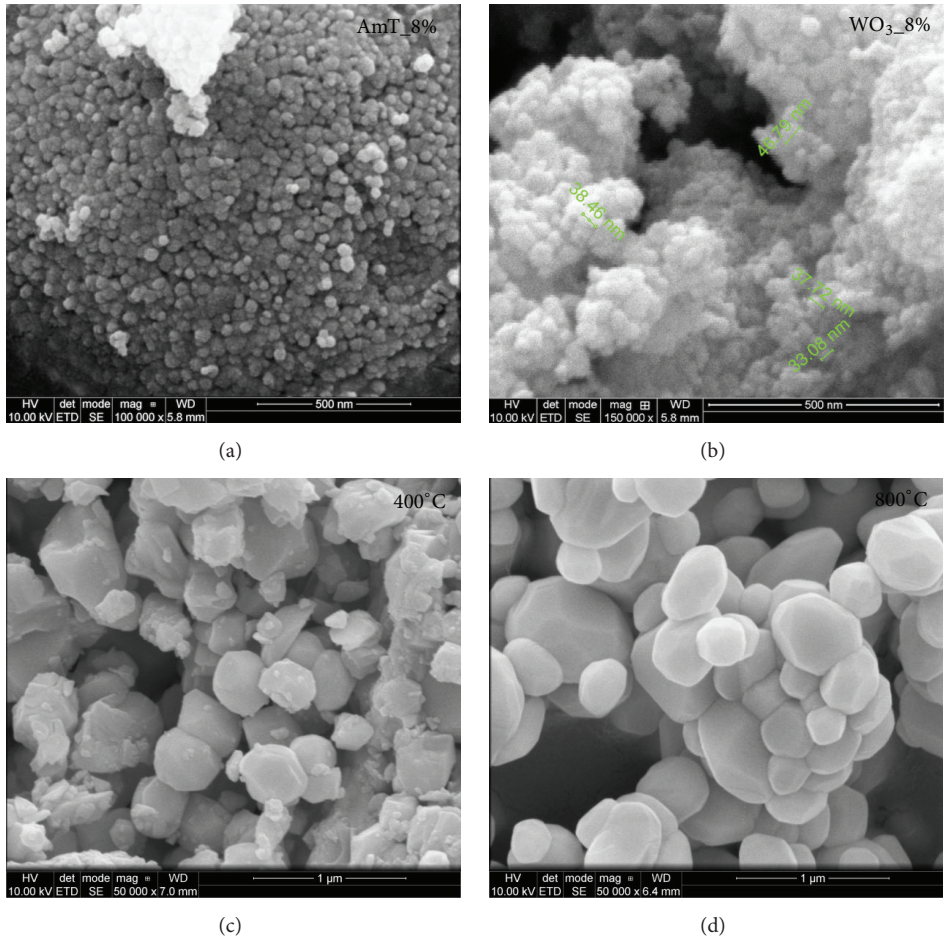

Figure 4: SEM images for sample AmT_8%_400 (a) and for sample WO_3_8%_400 (b). The effect of calcination temperature on the structure of WO_3_8%_400 (c) and WO_3_8%_800 nanocomposites.

Table 2: The effect of calcination temperature on the content of amorphous and crystalline phases of WO_3/TiO_2 samples.

Sample	Calcination temperature (°C)	Crystalline phase content (%)	Amorphous phase content (%)
WO_3_8% (without heat treatment)	—	42	58
WO_3_8%_400	400	39	60
WO_3_8%_500	500	77	23
WO_3_8%_600	600	76	22
WO_3_8%_700	700	75	25
WO_3_8%_800	800	80	20
WO_3_8%_900	900	82	18

temperature 500°C, regarding the morphological properties of the nanocomposites. The hydrothermal reaction time and temperature as well as duration of the calcination may affect the further reduction in the amount of amorphous phase in the WO_3/TiO_2 structure. Therefore, the further optimization of the conditions of hydrothermal reaction of WO_3/TiO_2 coupled photocatalysts should be continued and correlated with amorphous and crystalline phase content.

3.3. Microscopic Analysis. Microstructure of obtained nanocomposites and their surface morphology were studied by SEM equipped with EDS. SEM analyses of WO_3/TiO_2 sample containing the same amount of tungsten trioxide but obtained by generating in situ WO_3 particles from WO_3 precursor (AmT) during preparation of nanocomposites (a) and using commercial WO_3 nanoparticles (b) are presented in Figure 4. Both samples have similar spherical particles shape and size in the range from 30 nm to 70 nm. The particles form loose aggregates with a significant porosity. Figures 4(c) and 4(d) show that annealing at 800°C increases the crystallinity of WO_3 nanoparticles compared to WO_3/TiO_2 sample calcined at 400°C. Sample calcinated at 800°C comprises well-developed crystals of WO_3/TiO_2 compared to that calcinated at 400°C with 3-fold lower crystallinity and higher amorphous phase content. Therefore, it can be concluded that the calcination temperature is crucial in the formation of particular morphology of spherical WO_3 nanoparticles. The tungsten content estimated with SEM-EDS for both

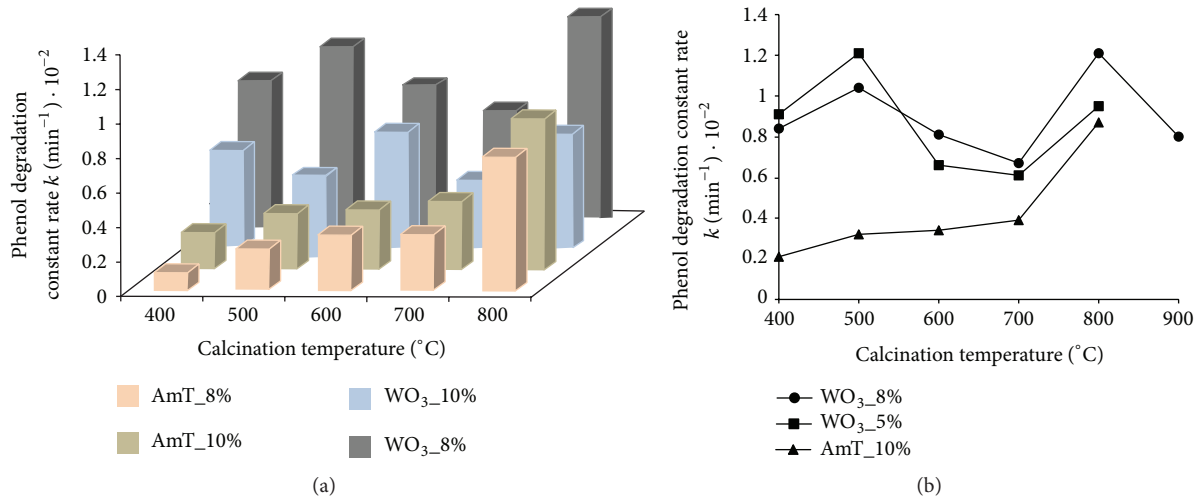

FIGURE 5: Kinetics of phenol degradation for samples AmT_8%, AmT_10%, WO_3_10%, and WO_3_8% under UV-Vis light. Experimental conditions: light source: Xe lamp, irradiation flux 24 mW/cm^2, phenol initial concentration: 0.2 mM, $m(TiO_2) = 0.05$ g, and $T = 15$°C. The effect of calcination temperature for the most active samples WO_3_8%, WO_3_5%, and AmT_10% (b).

WO_3_8%_400 and WO_3_8%_800 samples varied between 1 and 2 at.%. For sample WO_3_8%_800 the measured amount of O was 78.6 at.%, Ti was 20 at.%, and W was 1.4 at.%. The atomic percent amounts of the species detected by EDX indicate a W/Ti atomic ratio equal to 0.27, which confirms the W nominal amount assessed in the preparation procedure. These results confirm that tungsten is present at the surface regions of the TiO_2 nanoparticles, although a minor incorporation into the TiO_2 lattice cannot be excluded and suggests the formation of WO_3 microdomains that create a structure in WO_3/TiO_2 rather than producing of TiO_2 doping.

3.4. Photocatalytic Activity of WO_3/TiO_2 Nanocomposites. The kinetics of phenol photodegradation in the presence of obtained WO_3/TiO_2 nanoparticles are shown in Figure 5 and the determined rate constants are also included in Table 1. The apparent rate constants of the first-order kinetics of phenol photodegradation increased from $0.06 \cdot 10^{-2}$ min^{-1} to $1.27 \cdot 10^{-2}$ min^{-1} for AmT_3%_400 and WO_3_8%_800, respectively. An increase in tungsten(VI) oxide content from 3 to 10 mol% for samples obtained using ammonium metatungstate (AmT) as WO_3 precursor resulted in enhancement of the photocatalytic activity under UV-Vis light irradiation. Moreover, as shown in Figure 5(a), the photocatalytic activity strongly depends on WO_3 source and calcination temperature. Phenol degradation rate constant for the most active sample WO_3_8%_800 increased about 1.6 times reaching $1.27 \cdot 10^{-2}$ min^{-1} compared to the sample AmT_8%_800 with the highest activity among WO_3/TiO_2 photocatalysts containing 8 mol% nominal value of tungsten(VI) oxide.

As shown in Figure 5(b), an increase of the calcination temperature from 400°C to 500°C resulted in an increase in photoactivity of the most active samples WO_3_8%, WO_3_5%, and AmT_10% and then decreased for the WO_3/TiO_2 nanocomposites obtained using commercial WO_3 particles (WO_3_5% and WO_3_8% series) and calcinated at 600°C and 700°C. The increase of photoactivity for those samples calcinated above 400°C can be correlated with 3-fold lower amount of amorphous phase in the structure of photocatalyst. Ohtani et al. reported the results of photocatalytic activity of anatase and amorphous TiO_2 and stated that amorphous titania contains imperfections, for example, impurities, dangling bonds, or microvoids, which lead to electronic states in the band gap, and acts as a recombination of charge carriers. Therefore, the photocatalytic activity of anatase crystallites is improved further by the heat treatment [19].

After annealing at 600°C samples with predominantly anatase structures were produced in which the contribution of the rutile phase can become more dominant by further increasing the annealing temperature. However, the highest photoactivity was observed for the sample containing 8 mol% of WO_3 calcined at 800°C (namely, 8%_WO_3_800). Further increase in annealing temperature to 900°C resulted in a drop of photoactivity from $1.27 \cdot 10^{-2}$ min^{-1} to $0.81 \cdot 10^{-2}$ min^{-1} for the sample WO_3_8% calcinated at 800°C and 900°C, respectively. The decrease of photoactivity above the optimal calcination temperature results from an increase in number of defects in the oxide structure, acting as charge carriers recombination centers [24].

4. Conclusions

The effect of annealing temperature is confirmed by the XRD, microscopy, and photocatalytic analysis. Increase in the calcination temperature resulted in increased clearly crystallite WO_3 content in the WO_3/TiO_2 nanocomposites structure, as well as decrease of WO_3/TiO_2 optical band gap energies due to incorporation of tungsten(VI) oxide into the structure of TiO_2. Moreover, an increase in the calcination temperature affects the increase in the amount of crystalline phase and reduction in the amount of amorphous phase in the nanocomposite structure. Therefore, taking into account the morphological properties of as-prepared WO_3/TiO_2

nanocomposites the calcination should proceed at 500°C. The annealing of WO_3/TiO_2 nanocomposites above 400°C increases the crystallinity of WO_3 nanoparticles and improves photoinduced charge carriers separation. The best photocatalytic activity revealed samples containing 5 mol% and 8 mol% of WO_3 and calcinated at temperature 500°C and 800°C. The results of photodecomposition of phenol in aqueous solution using WO_3/TiO_2 nanocomposites under UV-Vis light irradiation indicated effect of tungsten(VI) oxide source and amount as well as the calcination temperature of the photocatalyst on the process efficiency.

Competing Interests

The authors declare that they have no competing interests.

References

[1] L. Rizzo, J. Koch, V. Belgiorno, and M. A. Anderson, "Removal of methylene blue in a photocatalytic reactor using polymethylmethacrylate supported TiO_2 nanofilm," *Desalination*, vol. 211, no. 1–3, pp. 1–9, 2007.

[2] N. Daneshvar, D. Salari, and A. R. Khataee, "Photocatalytic degradation of azo dye acid red 14 in water: investigation of the effect of operational parameters," *Journal of Photochemistry and Photobiology A: Chemistry*, vol. 157, no. 1, pp. 111–116, 2003.

[3] F. Benoit-Marquié, U. Wilkenhöner, V. Simon, A. M. Braun, E. Oliveros, and M.-T. Maurette, "VOC photodegradation at the gas-solid interface of a TiO_2 photocatalyst: part I: 1-butanol and 1-butylamine," *Journal of Photochemistry and Photobiology A: Chemistry*, vol. 132, no. 3, pp. 225–232, 2000.

[4] Y. Yao, T. Ochiai, H. Ishiguro, R. Nakano, and Y. Kubota, "Antibacterial performance of a novel photocatalytic-coated cordierite foam for use in air cleaners," *Applied Catalysis B: Environmental*, vol. 106, no. 3-4, pp. 592–599, 2011.

[5] A. V. Emeline, V. N. Kuznetsov, V. K. Ryabchuk, and N. Serpone, "On the way to the creation of next generation photoactive materials," *Environmental Science and Pollution Research*, vol. 19, no. 9, pp. 3666–3675, 2012.

[6] M. Anpo, "Use of visible light. Second-generation titanium oxide photocatalysts prepared by the application of an advanced metal ion-implantation method," *Pure and Applied Chemistry*, vol. 72, no. 9, pp. 1787–1792, 2000.

[7] T. Ohno, T. Mitsui, and M. Matsumura, "Photocatalytic activity of S-doped TiO_2 photocatalyst under visible light," *Chemistry Letters*, vol. 32, no. 4, pp. 364–365, 2003.

[8] E. Kowalska, H. Remita, C. Colbeau-Justin, J. Hupka, and J. Belloni, "Modification of titanium dioxide with platinum ions and clusters: application in photocatalysis," *The Journal of Physical Chemistry C*, vol. 112, no. 4, pp. 1124–1131, 2008.

[9] G. Xin, W. Guo, and T. Ma, "Effect of annealing temperature on the photocatalytic activity of WO_3 for O_2 evolution," *Applied Surface Science*, vol. 256, no. 1, pp. 165–169, 2009.

[10] Z.-G. Zhao and M. Miyauchi, "Nanoporous-walled tungsten oxide nanotubes as highly active visible-light-driven photocatalysts," *Angewandte Chemie—International Edition*, vol. 47, no. 37, pp. 7051–7055, 2008.

[11] M. Grandcolas, T. Cottineau, A. Louvet, N. Keller, and V. Keller, "Solar light-activated photocatalytic degradation of gas phase diethylsulfide on WO_3-modified TiO_2 nanotubes," *Applied Catalysis B: Environmental*, vol. 138-139, pp. 128–140, 2013.

[12] S. Bai, H. Liu, J. Sun et al., "Improvement of TiO_2 photocatalytic properties under visible light by WO_3/TiO_2 and MoO_3/TiO_2 composites," *Applied Surface Science*, vol. 338, pp. 61–68, 2015.

[13] K. K. Akurati, A. Vital, J.-P. Dellemann et al., "Flame-made WO_3/TiO_2 nanoparticles: relation between surface acidity, structure and photocatalytic activity," *Applied Catalysis B: Environmental*, vol. 79, no. 1, pp. 53–62, 2008.

[14] M. R. Hoffmann, S. T. Martin, W. Choi, and D. W. Bahnemann, "Environmental applications of semiconductor photocatalysis," *Chemical Reviews*, vol. 95, no. 1, pp. 69–96, 1995.

[15] Y. T. Kwon, K. Y. Song, W. I. Lee, G. J. Choi, and Y. R. Do, "Photocatalytic behavior of WO_3-loaded TiO_2 in an oxidation reaction," *Journal of Catalysis*, vol. 191, no. 1, pp. 192–199, 2000.

[16] K. Y. Song, M. K. Park, Y. T. Kwon, H. W. Lee, W. J. Chung, and W. I. Lee, "Preparation of transparent particulate MoO_3/TiO_2 and WO_3/TiO_2 films and their photocatalytic properties," *Chemistry of Materials*, vol. 13, no. 7, pp. 2349–2355, 2001.

[17] S. A. K. Leghari, S. Sajjad, F. Chen, and J. Zhang, "WO_3/TiO_2 composite with morphology change via hydrothermal template-free route as an efficient visible light photocatalyst," *Chemical Engineering Journal*, vol. 166, no. 3, pp. 906–915, 2011.

[18] H. Zhang, J. Han, X. Niu, X. Han, G. Wei, and W. Han, "Study of synthesis and catalytic property of WO_3/TiO_2 catalysts for NO reduction at high temperatures," *Journal of Molecular Catalysis A: Chemical*, vol. 350, no. 1-2, pp. 35–39, 2011.

[19] B. Ohtani, Y. Ogawa, and S.-I. Nishimoto, "Photocatalytic activity of amorphous-anatase mixture of titanium(IV) oxide particles suspended in aqueous solutions," *Journal of Physical Chemistry B*, vol. 101, no. 19, pp. 3746–3752, 1997.

[20] V. Rajani and N. Vijayan, "Isolation and identification of phenol degrading bacteria from effluent treatment plant of textile industry in Kerala," *International Journal of Pure & Applied Bioscience*, vol. 3, no. 5, pp. 88–94, 2015.

[21] C. Shifu, C. Lei, G. Shen, and C. Gengyu, "The preparation of coupled WO_3/TiO_2 photocatalyst by ball milling," *Powder Technology*, vol. 160, no. 3, pp. 198–202, 2005.

[22] V. Iliev, D. Tomova, S. Rakovsky, A. Eliyas, and G. Li Puma, "Enhancement of photocatalytic oxidation of oxalic acid by gold modified WO_3/TiO_2 photocatalysts under UV and visible light irradiation," *Journal of Molecular Catalysis A: Chemical*, vol. 327, no. 1-2, pp. 51–57, 2010.

[23] L. Yang, Z. Si, D. Weng, and Y. Yao, "Synthesis, characterization and photocatalytic activity of porous WO_3/TiO_2 hollow microspheres," *Applied Surface Science*, vol. 313, pp. 470–478, 2014.

[24] S. Y. Chai, Y. J. Kim, and W. I. Lee, "Photocatalytic WO_3/TiO_2 nanoparticles working under visible light," *Journal of Electroceramics*, vol. 17, no. 2–4, pp. 909–912, 2006.